Photon energy dependence of angle-resolved photoemission spectroscopy in graphene

Pourya Ayria,[1,*] Ahmad R. T. Nugraha,[1] Eddwi H. Hasdeo,[1] Thomas R. Czank,[1] Shin-ichiro Tanaka,[2] and Riichiro Saito[1]
[1]*Department of Physics, Tohoku University, Sendai 980-8578, Japan*
[2]*The Institute of Scientific and Industrial Research, Osaka University, Osaka 567-0047, Japan*
(Received 27 July 2015; revised manuscript received 15 October 2015; published 24 November 2015)

The photon energy dependence of angle-resolved photoemission spectroscopy (ARPES) in graphene is investigated experimentally and theoretically. By applying light with energy of around 46 eV, we found an unexpected increase in the ARPES relative intensity of graphene for the p branch (ARPES spectra brightened by the p-polarized light) with respect to the s branch (those brightened by the s-polarized light). The origin of the enhanced p-branch intensity is explained by first-principles calculations, in which we show (1) the optical dipole vector as a function of final-state energies of the excited electron, (2) the absorption intensity as a function of the incident light angle, and (3) the symmetry of the initial and the final states. The calculated results imply that the dipole vector of the excited electron near 46 eV has an exceptionally large component in the normal direction of the graphene surface compared to that within the graphene plane, which could be the main reason for the enhancement of the p-branch intensity.

DOI: 10.1103/PhysRevB.92.195148 PACS number(s): 73.22.Pr, 71.15.Mb, 79.60.−i

I. INTRODUCTION

In the last decade, graphene and graphene-based atomic layer materials have provided us with intensive nanoscale research in terms of their novel electronic structures and advanced applications [1–5]. In order to understand various phenomena in these materials, it is necessary for us to study their electronic structure. With this regard, angle-resolved photoemission spectroscopy (ARPES) is a useful method to observe the valence electronic energy dispersion of the solids. In ARPES, if the energy of photoexcited electrons surpasses the work function of the sample, the photoelectrons are ejected from the surface of a material. The kinetic energy and momentum of the photoelectron are observed by an analyzer from which we can directly get information on the electron-energy dispersion of the valence energy bands [6].

The electron-energy band structure of graphene can be observed by applying different light polarizations. When the incident light polarization is parallel or perpendicular to a plane that includes the incident light and ejected photoexcited electron, they are named as p-polarized or s-polarized light, respectively [7]. Some previous studies showed that, in the ARPES spectra of graphene, π and π^* bands near the Dirac point along the Γ–K direction are brightened by the p- and s-polarized light, respectively [8–11]. On the other hand, for the direction along K–M, the π and π^* bands are brightened by the s- and p-polarized light, respectively. The energy band brightened by the p-polarized light is referred to as the p branch, while that brightened by the s-polarized light is called the s branch. Such polarization dependence is known as the electronic chirality or chiral phenomenon of graphene in ARPES spectra.

In ARPES, propagating directions of the incident light and the ejected photoexcited electron makes a plane which is important to discuss the symmetry of graphene [7]. Some researchers in the previous studies explained the chiral phenomenon in graphene by considering the interference of electron wave functions for A and B atoms in the initial states [8–10]. They calculated the electron-photon matrix elements in the presence of p- or s-polarized light for the ARPES intensity and they considered the wave functions of the final states as a single plane wave, which has even symmetry with respect to the plane of incident light and ejected electrons. Since the dependence of the electron-photon matrix elements on the final-state wave functions was not considered to explain the chiral phenomenon, they refer to the phenomenon only as the initial state effects on the electron-photon matrix elements. However, Grüneis *et al.* showed much earlier that, in the calculation of a $\pi - \pi^*$ optical transition, the direction of the electron-photon dipole vectors critically depend on the final states [12]. In particular, the direction of the dipole vectors will change for different final states which are independent of light polarization. Thus, studying the final-state effects on the electron-photon matrix elements is essential for ARPES spectra.

To consider the final-state effects experimentally, we can apply a variation in the photon energy. Gierz *et al.* showed that by applying different photon energies in ARPES measurements of graphene, the s-polarized light with energy of around 52 eV can illuminate both bands in the direction of Γ–K and K–M due to the change of the final states [11,13]. Furthermore, they used circularly polarized light to observe the polarization dependence of the ARPES spectra for different photon energies [14]. Their experimental results show that the ARPES intensity for left and right circular polarization becomes almost the same near 46-eV photon energy. However, their theoretical approach did not reproduce the experimental results [14].

Motivated by the above-mentioned issues, here we combine experimental and theoretical approaches to clarify the photon energy and polarization dependence of the ARPES spectra in graphene. Our experimental observations and theoretical calculations reveal that the intensity of the p branch near photon energy $\hbar\omega = 46$ eV significantly increases even when the almost s-polarized light with a small fraction of the p-polarized light is applied. We find that the dipole vector in the direction normal to the graphene surface is quite large compared with that in the direction of the in-plane graphene

*pourya@flex.phys.tohoku.ac.jp

surface. This result can be the origin of the p-branch intensity enhancement near $\hbar\omega = 46$ eV. Based on the group theory analysis, we can also explain the chiral phenomenon of graphene.

This paper is organized as follows. In Sec. II we describe the geometry and formulation of the ARPES intensity within the dipole approximation. In Sec. III, the ARPES experimental observation in graphene for different photon energies is shown. In Sec. IV, the chiral dependence of the graphene band structure near the Dirac point for the s- and p-polarized light in the ARPES is obtained by the group theory. In Sec. V, the electron-photon matrix element effect on the ARPES intensity in graphene is discussed experimentally and theoretically. Finally, we give a summary in Sec. VI.

II. CALCULATION METHODS

ARPES intensity is proportional to the number of photoexcited electrons, which is proportional to the square of the electron-photon matrix element. Here, we briefly show how to calculate the electron-photon matrix element. The Hamiltonian H for an electron with mass m and charge $-e$ under an electromagnetic field with vector potential $\mathbf{A}(t)$ is given by

$$H = \frac{1}{m}[-i\hbar\nabla + e\mathbf{A}(t)]^2 + V(\mathbf{r}), \tag{1}$$

where $V(\mathbf{r})$ is a potential of the material. The vector potential $\mathbf{A}(t)$ in the vacuum can be written in terms of incident light intensity I and the unit vector of the electric field $\mathbf{P}$ as

$$\mathbf{A}(t) = \frac{-i}{\omega}\sqrt{\frac{I}{c\varepsilon_0}}\exp(-i\omega)\mathbf{P}, \tag{2}$$

where ω is the angular frequency of a photon, ε_0 is the dielectric constant of the vacuum, and c is the velocity of the light. Within the dipole approximation for Eq. (1), we neglect quadratic terms in $\mathbf{A}(t)$ and use the Coulomb gauge $\nabla\cdot\mathbf{A}(t) = 0$. Then the perturbation Hamiltonian $H_{\rm opt}$ is given by

$$H_{\rm opt} = \frac{ie\hbar}{m}\mathbf{A}(t)\cdot\nabla. \tag{3}$$

The electron-photon matrix element is defined by

$$M_{\rm opt}(\mathbf{k}_i,\mathbf{k}_f) = \langle\Psi^f(\mathbf{k}_f,\mathbf{r})|H_{\rm opt}|\Psi^i(\mathbf{k}_i,\mathbf{r})\rangle, \tag{4}$$

where $\Psi^i(\mathbf{k}_i,\mathbf{r})$ and $\Psi^f(\mathbf{k}_f,\mathbf{r})$ are the wave functions of an initial and a final state, respectively, and $\mathbf{k}$ is the wave vector. When we assume that $\mathbf{A}$ is a slowly changing function of $\mathbf{r}$ compared with Ψ^i or Ψ^f, the electron-photon matrix element can be written as [12]

$$M_{\rm opt}(\mathbf{k}_i,\mathbf{k}_f) \propto \mathbf{A}\cdot\mathbf{D}(\mathbf{k}_i,\mathbf{k}_f), \tag{5}$$

where the dipole vector $\mathbf{D}(\mathbf{k}_i,\mathbf{k}_f)$ is defined as

$$\mathbf{D}(\mathbf{k}_i,\mathbf{k}_f) = \langle\Psi^f(\mathbf{k}_f,\mathbf{r})|\nabla|\Psi^i(\mathbf{k}_i,\mathbf{r})\rangle. \tag{6}$$

In ARPES, we change the angle of incident light ψ with respect to normal to the sample, [see Fig. 1(a)]. The relationship between the angle of incident light and the transmitted light in the sample is given by the Fresnel equation [15–17]. In the Fresnel equation, for a given vector potential of incident light $\mathbf{A}_i$ in the vacuum, the vector potential of transmitted light $\mathbf{A}^t$ in the graphene with a dielectric function $\varepsilon(\omega) = \varepsilon_1(\omega) + i\varepsilon_2(\omega)$ is given as follows [15–17]:

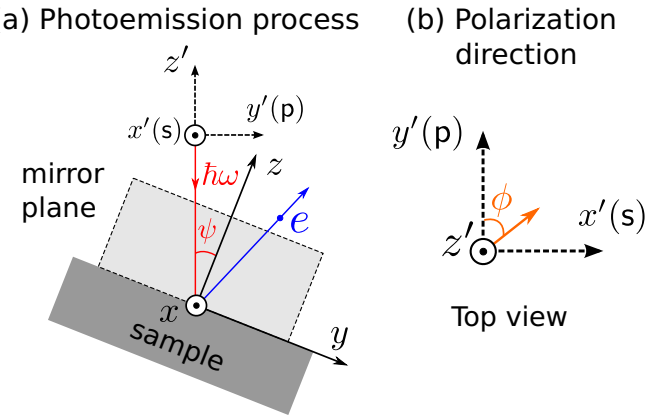

FIG. 1. (Color online) (a) Geometry of photoemission process. Incident photons with energy $\hbar\omega$ are shown by red arrow. We can define a mirror plane which contains the incident light ($-z'$ axis), the electrons ejected from the surface (blue arrow), and an axis (z axis) normal to the graphene surface. The angle between incident light and the z axis is denoted by ψ. (b) From the z' axis we see that the light polarization angle can be defined by an angle ϕ in the $x'y'$ plane and measured by the y' axis. $\phi = 0^\circ$ and $\phi = 90^\circ$ corresponds to the p and s polarization, respectively.

$$\begin{aligned}
A^t_x &= \frac{2\cos\psi\sin\phi}{\cos\psi + \sqrt{\varepsilon(\omega) - \sin^2\psi}}|\mathbf{A}_i|,\\
A^t_y &= \frac{2\sqrt{\varepsilon - \sin^2\psi}\cos\psi\cos\phi}{\varepsilon(\omega)\cos\psi + \sqrt{\varepsilon(\omega) - \sin^2\psi}}|\mathbf{A}_i|,\\
A^t_z &= \frac{2\cos\psi\sin\psi\cos\phi}{\varepsilon(\omega)\cos\psi + \sqrt{\varepsilon(\omega) - \sin^2\psi}}|\mathbf{A}_i|,
\end{aligned} \tag{7}$$

where $A^t_{x,y,z}$ are the x, y, and z component of $\mathbf{A}^t$, and ϕ is the light polarization angle measured from the y' axis as shown in Fig. 1(b). In particular, $\phi = 0^\circ$ and $\phi = 90^\circ$ correspond to the p polarization and s polarization, respectively. As shown in Fig. 1(a), we define a mirror plane which consists of z' (red line) and z axes and the direction of an ejected electron (blue line). The dielectric function of graphene is approximated by $\varepsilon \approx 0.9 + 0.0001i$ for photon energies larger than 20 eV [18,19].

To consider the final-state effects on the the matrix elements, we expand the wave functions of the initial states and final states in terms of plane waves,

$$\begin{aligned}
\Psi^i(\mathbf{k}_i,\mathbf{r}) &= \sum_{\mathbf{G}} C^i_{\mathbf{G}}(\mathbf{k}_i)\exp\left(i(\mathbf{k}_i + \mathbf{G})\cdot\mathbf{r}\right),\\
\Psi^f(\mathbf{k}_f,\mathbf{r}) &= \sum_{\mathbf{G}} C^f_{\mathbf{G}}(\mathbf{k}_f)\exp\left(i(\mathbf{k}_f + \mathbf{G})\cdot\mathbf{r}\right),
\end{aligned} \tag{8}$$

where $\mathbf{G}$ represents the reciprocal lattice vectors of graphene and $C^{i,f}_{\mathbf{G}}(\mathbf{k})$ the plane-wave coefficients. We set the upper limit of the photon energy as 60 eV. In this case, the optical transition occurs vertically in the $\mathbf{k}$ space, that is, $\mathbf{k}_i \approx \mathbf{k}_f = \mathbf{k}$. It should be noted that this assumption is no longer valid in the x-ray photoelectron spectroscopy (XPS) measurement [20].

Inserting Eq. (8) into Eq. (6), we obtain

$$\mathbf{D}(\mathbf{k}) = \sum_{\mathbf{G}} C^{f*}_{\mathbf{G}}(\mathbf{k}) C^{i}_{\mathbf{G}}(\mathbf{k})(\mathbf{k}+\mathbf{G}). \quad (9)$$

The ARPES intensity I as a function of wave vectors $\mathbf{k}$ and photon energy $\hbar\omega$ can be calculated by using Fermi's golden rule as follows [21]:

$$I(\mathbf{k},\hbar\omega) \propto \sum_{i} \left| \sum_{f} \mathbf{M}_{\mathrm{opt}}(\mathbf{k}) \right|^2 \delta(E_f - E_i - \hbar\omega), \quad (10)$$

where E_i and E_f are the energies of the initial and final states of the electron, respectively, and the Dirac δ function implies an energy conservation. The absolute value is taken after the summation of the final states to assure that all interference phenomena for a given initial state are included [22]. In our calculations, the δ function is replaced by a Lorentzian, having a finite half-width of energy 0.6 eV which is obtained by fitting to experimental spectra. The excited electrons can escape from the surface if E_f is larger than the work function of graphene, $\phi_{\mathrm{wf}} = 4.5$ eV [23].

We calculate the wave-function coefficients of graphene in terms of plane waves within a first-principles approach as implemented in the QUANTUM ESPRESSO package [24]. We adopt the norm-conserving pseudopotential with Perdew-Zunger (local-density approximation) exchange-correlation scalar relativistic functional. The kinetic energy cutoff is taken as 60 Ry for each atom, and the kinetic energy cutoff for density potential is set to 600 Ry in order to verify the convergence of all wave functions. The k-point mesh grid for self-consistent calculation is $52 \times 52 \times 1$ in the graphene Brillouin zone. The lattice parameter of graphene is 4.602 a.u., and the lattice constant for the unit cell normal to the graphene planes is taken as $c/a = 10$ to avoid interlayer interaction.

In Fig. 2 we show the calculated energy-band structure of graphene along the high-symmetry points in the first Brillouin zone of graphene. The energy dispersions are calculated up to 70 eV above the Dirac point. As seen in Fig. 2, the energy bands of graphene cross each other at around 20 and 50 eV near the K point, consistent with some earlier studies [9,11].

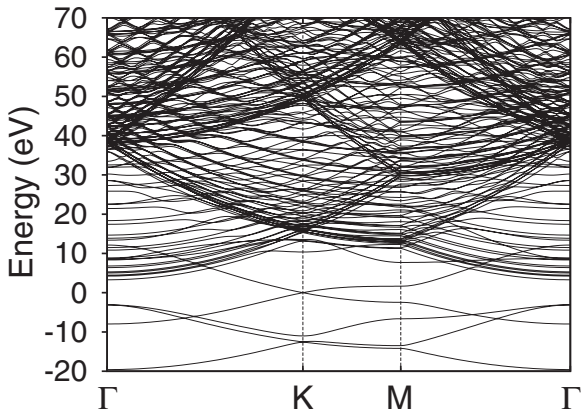

FIG. 2. The electronic energy dispersion relation of graphene obtained from first-principles calculation is plotted along the high-symmetry points Γ–K–M up to 70 eV.

III. EXPERIMENTAL METHODS

The single-layered graphene sample, epitaxially grown on a SiC substrate, was manufactured by Graphene Platform, Inc. (Tokyo, Japan). The sample was cleaned by heating at 900 °C at pressures less than 2×10^{-7} Pa. The temperature and the pressure during the ARPES measurements were 100 K and 7×10^{-9} Pa, respectively.

All the ARPES measurements were carried out on the beamline BL-1 of the synchrotron radiation facility at Hiroshima University (HiSOR) [25,26]. The beamline consists of a linear undulator, a spherical-grating grating monochromator of Dragon type, and the experimental chamber equipped with a hemispherical electron-energy analyzer (R4000, VG-Scienta, Sweden) and a liquid-He-flow-type, five-axis goniometer (i-GONIO LT, R-dec Co., Japan) that mounts the sample. The experimental chamber can be rotated around the monochromized photon beam which is polarized along the horizontal plane, and thus the polarization plane with respect to the sample surface can be changed to any angle. The angle between the center of the acceptance angle of the electron analyzer and the photon beam was fixed at 50°. The ARPES measurements were performed with energy and angular resolutions of 0.25 eV and 0.02°, respectively.

In order to extract the experimental intensities, we first obtained the momentum distribution curves using the photoelectron intensity integrated within the energy window of 0.25 eV centered at the Fermi level. Then these curves are analyzed by the least-squares curve fitting using two pseudo-Voigt functions with a linear background. We used the area intensities of the obtained pseudo-Voigt functions.

IV. SYMMETRY SELECTION RULE FOR THE ELECTRON-PHOTON INTERACTION

In Figs. 3(a)–3(c), we show the experimental ARPES spectra near the Dirac point for several polarization angles in which the photon energy is fixed at $\hbar\omega = 50$ eV and the incident angle is $\psi = 18°$. The polarization angles $\phi = 0°$ and $\phi = 90°$ in Figs. 3(a) and 3(c) correspond to the case of pure p- and s-polarized light, respectively, while $\phi = 78°$ in Fig. 3(b) has some contributions from both the p- and s-polarized light. The π and π^* bands of graphene along the Γ–K direction near the Dirac point are brightened by the p- and s-polarized

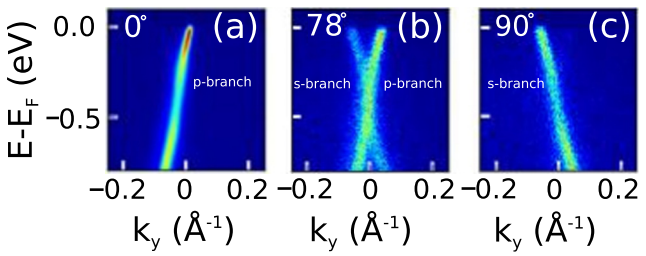

FIG. 3. (Color online) ARPES spectra of graphene near the Dirac point (K) as a function of the wave vector for (a) the p-polarized light at $\phi = 0°$, (b) the $\phi = 78°$ polarized light, and (c) the s-polarized light at $\phi = 90°$. The photon energy is $\hbar\omega = 50$ eV, and the incident angle is $\psi = 18°$. In this case, $k_y = 0$ refers to the K point, and $k_y > 0$ ($k_y < 0$) is along the K–M (K–Γ) direction.

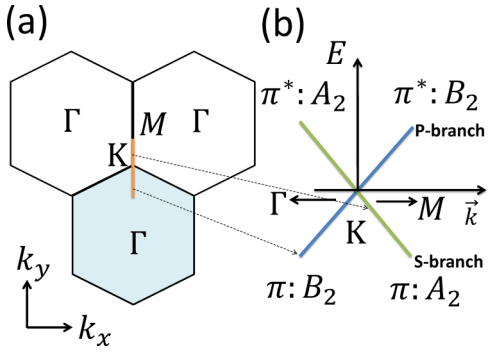

FIG. 4. (Color online) (a) Hexagonal Brillouin zone of graphene (shaded area). The ARPES calculation is performed near the K point along the line Γ–K and K–M, which is shown by the orange line. (b) The schematic linear band structure of graphene along Γ–K and K–M on the orange-colored line with their representation of point-group symmetry. The p-polarized light illuminates the blue energy band with B_2 symmetry and the s-polarized light illuminates the green energy band with A_2 symmetry.

light (in the case of n-doped graphene), as shown in Figs. 3(a) and 3(c), respectively. On the other hand, for the direction along K–M, the π and π^* bands are brightened by the s- and p-polarized light, respectively. In the case of other polarization angles which are not equal to $\phi = 0^\circ$ and $\phi = 90^\circ$, we might expect some brightening on either the p branch or the s branch, such as the one shown in Fig. 3(b). In order to explain the polarization dependence of the π and π^* bands near Dirac point, the symmetry of the wave function and electron-photon matrix element can be analyzed by the group theory [7,27].

The optical dipole selection rule imposes a nonzero matrix element for the transition which satisfies

$$\Gamma_o \subset \Gamma_f \otimes \Gamma_i, \tag{11}$$

where Γ_i, Γ_f, and Γ_o are, respectively, irreducible representations for the initial state, the final state of the electron wave function, and the x,y,z component of ∇ in Eq. (6). In the case of graphene, the point-group symmetry of wave functions along the Γ–K and K–M lines in Fig. 4(a) belongs to the C_{2v} point group [28–30]. The C_{2v} symmetry group has four irreducible representations $\{A_1, A_2, B_1, B_2\}$, as shown in Table I. According to the x,y,z coordinate in Fig. 4(a), the character table of C_{2v} is listed in Table I. Studying the symmetry of wave functions from first-principles calculation also indicates that there is a C_{2v} symmetry along the high-symmetry points of graphene near the Dirac point. The calculation shows that π and π^* bands of graphene along the Γ–K (K–M) line have B_2 (A_2) and A_2 (B_2) symmetry,

TABLE I. Character table of $C_{2v}(2mm)$ point group.

	E	C_2	$\sigma_v(xz)$	$\sigma_v'(yz)$	Bases
A_1	1	1	1	1	z, ∇_z
A_2	1	1	−1	−1	R_z
B_1	1	−1	1	−1	x, R_y, ∇_x
B_2	1	−1	−1	1	y, R_x, ∇_y

TABLE II. Product of C_{2v} representation, $\Gamma_f \otimes \Gamma_i$, with the initial states $\Gamma_i = \{A_2, B_2\}$ and the final state $\Gamma_f = \{A_1, B_2\}$.

	A_2	B_2
A_1	A_2	B_2
B_2	B_1	A_1

respectively. We give a schematic illustration for the symmetry of the wave function for each band in Fig. 4(b).

In ARPES, to have a nonzero matrix element, the integral of the $\langle \Psi^f | \mathbf{A} \cdot \mathbf{P} | \Psi^i \rangle$ must be an even function under reflection with respect to the mirror plane $\sigma_v'(yz)$, which was defined in Fig. 1. Moreover, the final state of the photoemitted electron, which is observable in the detector, must be an even function under reflection with respect to the mirror plane $\sigma_v'(yz)$ [6,7,9,31]. Hence, the final state can have either $\Gamma_f = A_1$ or B_2 symmetry. As a result, applying the p-polarized light, which has even symmetry with respect to $\sigma_v'(yz)$, brightens the π band along the Γ–K line and the π^* band along the K–M line with the same B_2 symmetry, comparable to the dipole vector in the direction of the y and z axes. On the other hand, the s-polarized light, which has odd symmetry with respect to $\sigma_v'(yz)$, brightens the π band along $K - M$ and the π^* band along Γ–K, corresponding to the dipole vector in the direction of the x axis [7,8]. Consequently, it can be the origin of the chiral dependence of the graphene bands near the Dirac point based on the calculation of the dipole vector. Therefore, applying p- or s-polarized light imposes a specific optical transition selection rule for the direction of the ejected electron, which is summarized in Table II. It is noted that in the product table (Table II), the A_2 symmetry does not refer any dipole vector direction.

V. ARPES NEAR THE FERMI LEVEL

To investigate the photon energy dependence of the graphene band ARPES intensity near the Fermi level, the ratio of the p-branch intensity to the s-branch intensity, I_p/I_s, is measured and calculated as a function of the photon energy at the Fermi energy, as shown in Fig. 5. (The I_s and I_p data from the experiment are shown in the inset of Fig. 5.) The Dirac point is located at about −0.4 eV below the Fermi energy. The polarization angle of light is fixed to be $\phi = 80^\circ$ and the incident angle is $\psi = 18^\circ$ for the photon energies in the range of $\hbar\omega = 42$–55 eV. In Fig. 5, the circles denote the experimental measurement, while the solid line denotes the calculated result. For the polarization angle $\phi = 80^\circ$, which is close to $\phi = 90^\circ$ (s-polarization), it is expected that the intensity of the s branch (A_2) is stronger than the p branch (B_2). However, our study shows that I_p increases more significantly near $\hbar\omega = 46$ eV rather than I_s. The drastic change in the intensity ratio I_p/I_s near $\hbar\omega = 46$ eV indicates such an enhancement of the p-branch intensity. Moreover, the experimental values of I_p/I_s are larger than the theoretical values. We believe that the discrepancy might arise from our experimental setup. Since the photoelectron detection efficiency for the s polarization is smaller than that for the p polarization, we expect that the detection

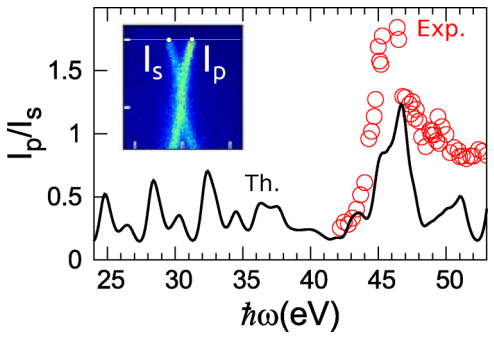

FIG. 5. (Color online) The ratio of the p-branch intensity to the s-branch intensity (I_p/I_s) is plotted as a function of photon energy $\hbar\omega$. The polarization angle is fixed at $\phi = 80°$. The open circles represent the experimental results, while the solid line represents the calculated I_p/I_s. The initial state $E_i = 0.4$ eV above the Dirac point is considered in the calculation. Both the experimental measurement and the theoretical calculation have a sharp peak at around 46 eV. (Inset) A particular example of how I_s and I_p (given by two dots) are taken along the s branch and p branch, respectively, at a given photon energy $\hbar\omega = 50$ eV.

efficiency of I_s is smaller than I_p. Particularly, when I_p increases, the difference between the experimental observation and the theoretical calculation also increases. A more detailed comparison between the experimental and calculation results are shown in Fig. 6. In Figs. 6(a) and 6(b), we show both I_p and I_s from experiment and calculation along Γ–K–M direction for several photon energies. For a given photon energy and polarization angle, I_p (I_s) is normalized to the maximum intensity values along the p branch (s branch), as shown in the inset of Fig. 5. The graphene is slightly

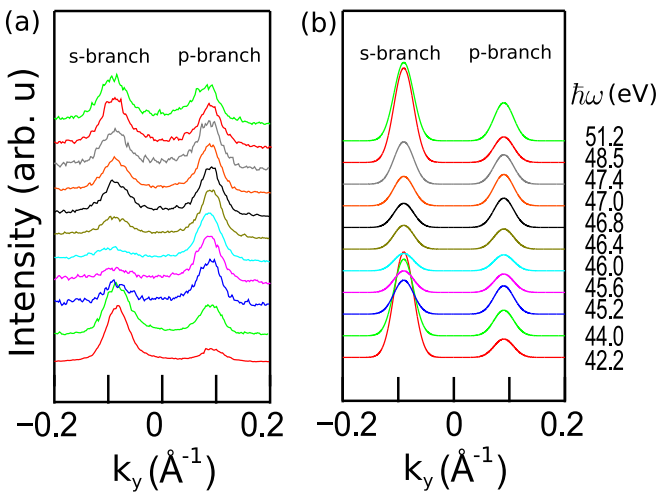

FIG. 6. (Color online) (a) Experimental and (b) calculated result of ARPES intensity (I_s and I_p) as a function of the wave vector k_y along the Γ–K–M direction for several photon energies. In both experimental measurement and theoretical calculation, the light polarization angle $\phi = 80°$ and the incident light angle $\psi = 18°$ are considered. For each photon energy, the I_s and I_p values are normalized to the largest value between the two. Furthermore, $\Delta k = 0.1$ Å is considered to plot the intensity as a function of the wave vector.

n doped because of charge transfer from the substrate. It can be seen that around the photon energy of 45–48 eV, the intensity of the p branch is higher than the intensity of the s branch.

The origin of enhanced intensity of the p branch near the photon energy $\hbar\omega = 46$ eV can then be explained by the electron-photon matrix element effects in graphene. Since the light incident angle is not perpendicular to the graphene surface, the vector potential outside of graphene relates to the transmitted vector potential into the graphene by Eq. (7), which is a function of the light incident angle and the dielectric function of graphene. The x,y,z component of the transmitted vector potential $\mathbf{A}$ is plotted as a function of incident light angle in Fig. 7 with the polarization angle of light $\phi = 80°$. It can be seen from Figs. 7(a) and 7(b) that the transmitted vector potential values for its x and y components are nonzero for $\psi = 0°$, and that their real and imaginary part are almost constant for $\psi < 30°$. Meanwhile, as shown in Fig. 7(c), the value of the z component of the transmitted vector potential is zero. Increasing the angle ψ will give a stronger A_z. The z component of the vector potential can enhance the intensity of the p branch (B_2) by brightening the z component of the

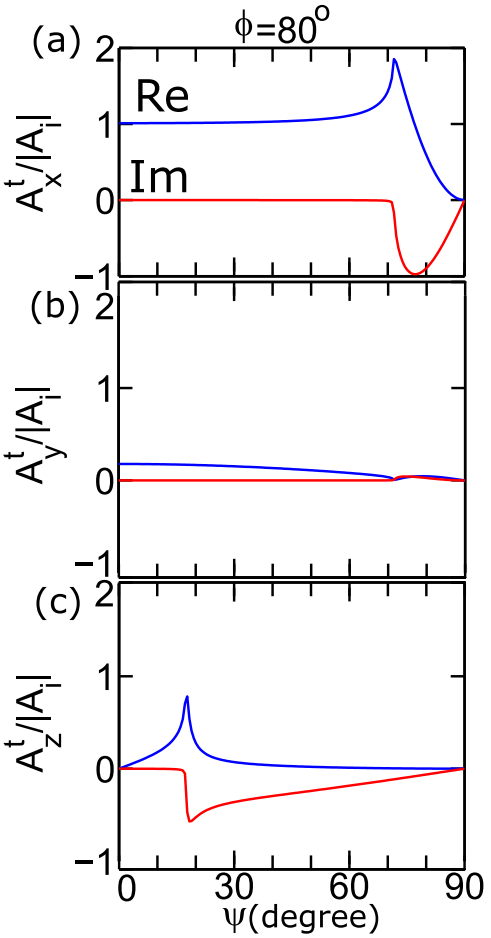

FIG. 7. (Color online) The real part and imaginary part of transmitted vector potential components: (a) A_x^t, (b) A_y^t, and (c) A_z^t, plotted as a function of the incidence angle ψ for the light polarization angle $\phi = 80°$.

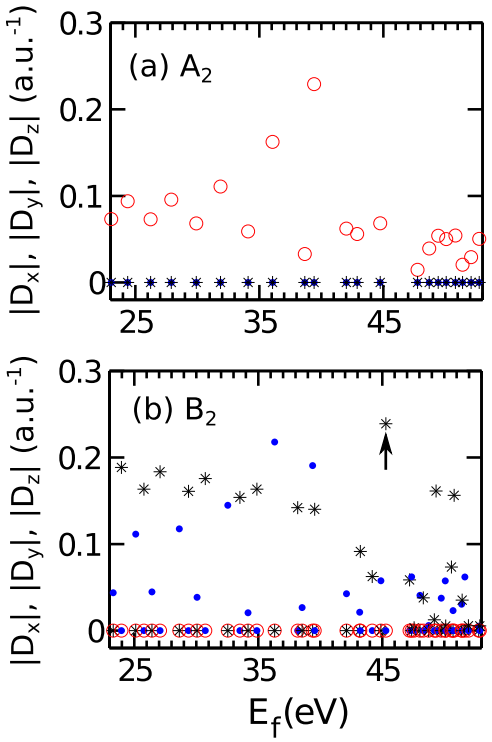

FIG. 8. (Color online) The x, y, and z components of the dipole vector, i.e., D_x (circles), D_y (dots), D_z (asterisks), plotted as a function of the energy of the final state E_f. The initial energy is taken to be $E_i = 0.4$ eV. In (a), the symmetry of the initial state along Γ–K is A_2, while in (b), the symmetry of the initial state along K–M is B_2. At around 46 eV, the strong z component of the dipole vector (as indicated by the arrow) results in a larger increase of the ARPES intensity of the p branch compared to that of the s branch in the presence of $\phi = 80^\circ$ light polarization.

dipole vector when the incident light is not normal to the surface.

To discuss the final-state dependence of the dipole vector, we plot in Fig. 8 the absolute value of the dipole vector components as a function of the final-state energy for different k points near the Dirac point along the Γ–K and K–M lines, which satisfies the explained symmetry rule discussed in the Sec. IV [32]. The initial state energy is $E_i = 0.4$ eV. The circles, dots, and asterisks in Fig. 8 denote the x, y, and z component of the dipole vector, i.e., D_x, D_y, and D_z, respectively. In our calculation, the direction of the dipole vector for $\pi - \pi^*$ transition ($B_2 - A_2$), D_x, is consistent with the results from Grüneis *et al.* for the dipole vectors along the Γ–K and K–M lines [12]. The dipole vector direction for each final state can be only in one direction of x, y, or z (see Fig. 8). Thus, the linearly polarized light cannot break the mirror-symmetry rules in the observation of photoexcited electrons, which is also confirmed by experimental measurement.

A large D_z is seen in Fig. 8 in the B_2 branch, around 46 eV, while the D_y values are very small near the photon energy $\hbar\omega = 46$ eV. Hence, the dependence D_y on the photon energy almost disappears, while D_z has large enhancement of the intensity for the p branch near $\hbar\omega = 46$ eV, as indicated by the arrow in Fig. 8(b). Therefore, when the z component of the vector potential has a non-negligible value, the z component of the dipole vector gives the contribution to enhancing the p branch. For this reason, the intensity of the p branch in graphene becomes much stronger than that of the s branch for the photon energy near $\hbar\omega = 46$ eV. Consequently, the origin of the strong peak observed at around 46 eV corresponds to the final-state effects on the electron-photon interaction in graphene. Moreover, since the direction of the dipole vector does not depend on the light polarization, our study suggests that near $\hbar\omega = 46$ eV the circular light dependency of ARPES intensity should almost disappear due to the small D_x and D_y values compared to the D_z value [14].

VI. SUMMARY

We have studied the photon energy dependence of ARPES intensity in graphene by ARPES measurement and first-principles calculation. Based on the measured and calculated ARPES intensity, we conclude that the intensity of the p branch in graphene near the photon energy $\hbar\omega = 46$ eV is stronger than that of the s branch, even when the polarized light is almost parallel to the s polarization. The origin of this observation is explained by the effects of the electron-photon matrix elements on the ARPES intensity in graphene. This study suggests that the presence of a larger z component of the dipole vector compared to the y components results in the enhanced intensity of the p branch near $\hbar\omega = 46$ eV. Furthermore, the chiral dependence in ARPES can be explained by the group theory. This approach also confirms that the p-polarized light brightens the band with B_2 symmetry, which has even symmetry with respect to the mirror plane, and s-polarized light brightens the band with A_2 symmetry, which has odd symmetry with respect to the mirror plane.

ACKNOWLEDGMENTS

The ARPES experiments were performed under the approval of the Hiroshima Synchrotron Radiation Center (Proposal No. 14-A-29). S.T. expresses sincere thanks to Dr. E. F. Schwier, Dr. H. Iwasawa, and Prof. K. Shimada of HiSOR for their kind assistance. S.T. thanks all the members of the HiSOR facility for their valuable help during the experiments. A.R.T.N. acknowledges financial support from the Leading Graduate School Program in Tohoku University and JSPS Grant No. 201303912. P.A., T.R.C., and E.H.H. are supported by a MEXT scholarship. R.S. acknowledges MEXT Grants No. 25107005 and No. 25286005.

[1] K. S. Novoselov, A. K. Geim, S. V. Morozov, D. Jiang, Y. Zhang, S. V. Dubonos, I. V. Grigorieva, and A. A. Firsov, Science **306**, 666 (2004).

[2] K. S. Novoselov, A. K. Geim, S. V. Morozov, D. Jiang, M. I. Katsnelson, I. V. Grigorieva, S. V. Dubonos, and A. A. Firsov, Nature (London) **438**, 197 (2005).

[3] A. Bostwick, T. Ohta, T. Seyller, K. Horn, and E. Rotenberg, Science **313**, 951 (2006).
[4] A. K. Geim, Science **324**, 1530 (2009).
[5] A. H. MacDonald and R. Bistritzer, Nature (London) **474**, 453 (2011).
[6] A. Damascelli, Z. Hussain, and Z. X. Shen, Rev. Mod. Phys. **75**, 473 (2003).
[7] H. Luth, *Surface and Interfaces of Solid Materials* (Springer-Verlag, Berlin, 1995).
[8] M. Mucha-Kruczynski, O. Tsyplyatyev, A. Grishin, E. McCann, V. I. Falko, A. Bostwick, and E. Rotenberg, Phys. Rev. B **77**, 195403 (2008).
[9] Y. Liu, G. Bian, T. Miller, and T.-C. Chiang, Phys. Rev. Lett. **107**, 166803 (2011).
[10] C. Hwang, C.-H. Park, D. A. Siegel, A. V. Fedorov, S. G. Louie, and A. Lanzara, Phys. Rev. B **84**, 125422 (2011).
[11] I. Gierz, J. Henk, H. Höchst, C. R. Ast, and K. Kern, Phys. Rev. B **83**, 121408 (2011).
[12] A. Grüneis, R. Saito, G. G. Samsonidze, T. Kimura, M. A. Pimenta, A. Jorio, A. G. Souza Filho, G. Dresselhaus, and M. S. Dresselhaus, Phys. Rev. B **67**, 165402 (2003).
[13] G. Malmstrom and J. Rundgren, J. Phys. C **13**, L61 (1980).
[14] I. Gierz, M. Lindroos, H. Höchst, C. R. Ast, and K. Kern, Nano Lett. **12**, 3900 (2012).
[15] M. Born and E. Wolf, *Principles of Optics* (Pergamon, Oxford, 1970).
[16] A. Gerlach, R. Matzdorf, and A. Goldmann, Phys. Rev. B **58**, 10969 (1998).
[17] F. Pforte, T. Michalke, A. Gerlach, A. Goldmann, and R. Matzdorf, Phys. Rev. B **63**, 115405 (2001).
[18] O. V. Sedelnikova, L. G. Bulusheva, and A. V. Okotrub, J. Chem. Phys. **134**, 244707 (2011).
[19] P. Rani, G. S. Dubey, and V. K. Jindal, Physica E **62**, 28 (2014).
[20] M. T. Chowdhury, R. Saito, and M. S. Dresselhaus, Phys. Rev. B **85**, 115410 (2012).
[21] S. Hufner, *Photoelectron Spectroscopy: Principles and Applications* (Springer-Verlag, Berlin, 1996).
[22] E. L. Shirley, L. J. Terminello, A. Santoni, and F. J. Himpsel, Phys. Rev. B **51**, 13614 (1995).
[23] G. Giovannetti, P. A. Khomyakov, G. Brocks, V. M. Karpan, J. van den Brink, and P. J. Kelly, Phys. Rev. Lett. **101**, 026803 (2008).
[24] P. Giannozzi *et al.*, J. Phys.: Condens. Matter **21**, 395502 (2009).
[25] K. Shimada, M. Arita, Y. Takeda, H. Fujino, K. Kobayashi, T. Narimura, H. Namatame, and M. Taniguchi, Surf. Rev. Lett. **09**, 529 (2002).
[26] H. Hayashi, K. Shimada, J. Jiang, H. Iwasawa, Y. Aiura, T. Oguchi, H. Namatame, and M. Taniguchi, Phys. Rev. B **87**, 035140 (2013).
[27] M. S. Dresselhaus, G. Dresselhaus, and A. Jorio, *Group Theory: Application to the Physics of Condensed Matter* (Springer-Verlag, Berlin, 2008).
[28] L. M. Malard, M. H. D. Guimaraes, D. L. Mafra, M. S. C. Mazzoni, and A. Jorio, Phys. Rev. B **79**, 125426 (2009).
[29] E. Kogan, V. U. Nazarov, V. M. Silkin, and E. E. Krasovskii, arXiv:1306.4084.
[30] E. Kogan and V. U. Nazarov, Phys. Rev. B **85**, 115418 (2012).
[31] S. K. Mahatha and K. S. R. Menon, Surf. Sci. **606**, 1705 (2012).
[32] J. Berkowitz, *Photoabsorption, Photoionization, and Photoelectron Spectroscopy* (Academic Press, New York, 1979).